

A Two-Stage Approach for Frequency Response Modeling and Metamaterial Rapid Design

Xiao Guo^{1, 2}, Chunlin Ji^{1, *}, Ruopeng Liu¹, and Tao Tang²

Abstract—We introduce a novel two-stage approach for rapid design of massive metamaterials (MTMs), where performances of thousands of microstructures require evaluation. In Stage I, an equivalent circuit model is synthesized via rational function modeling to represent the frequency response of MTMs microstructures. In Stage II, Gaussian process (GP) regression models are unitized to build the relation between the physical setting of the microstructure, including geometric design variables and incident angles of electromagnetic (EM) waves, and the representing parameters of the equivalent circuit model. As a consequence, the mapping from the microstructure physical parameters to the frequency response is easy to achieve and with high accuracy. We offer two metamaterial prototypes to illustrate that the proposed approach allows high efficiency in facilitating the design of massive MTMs. The experimental results demonstrate that our method is no longer limited by the complexity of microstructures and the spatial dispersion, induced by the variation of incident angle. We compare the accuracy of predicted responses against the reference data, and both examples yield average RMSE less than 0.05, which meets the requirements for many MTMs engineering applications.

1. INTRODUCTION

Metamaterials are artificially designed materials that consist of sub-wavelength microstructure unit cells which yield specific responses to the electromagnetic (EM) field applied, leading to extraordinary behaviors that cannot be achieved with natural materials [1, 2]. MTMs have drawn great interest toward achieving novel physics phenomenon and unique functionalities, including negative refractive indexes [1, 2] and perfect lensing [3, 4], whose realization requires careful design of the topology and geometric dimensions of their microstructures [5, 6].

In practice, the MTM design process is dominated by the speed of full-wave simulations where Maxwell's equations are solved typically using the finite integration technique (FIT) and finite element method (FEM). This commonly applied process suffers from repeated simulations in tailoring the macroscopic EM behavior of each particle. Moreover, the recent advance in electromagnetic technology demands that MTM microstructures of great complexity and variety in topology be integrated into the same system [5, 6], which are more expensive to run the simulation.

To provide an analytical expression of MTMs functional response, the Drude/Lorentz-type model, also known as the effective medium method, was proposed [7–9]. This approach approximates MTMs EM performances with two constitutive parameters, namely, effective permittivity and effective permeability which are retrieved from MTMs reflection and transmission coefficients, acquired at exact normal incidence. However, the spatial dispersion relies not only on the spatial distribution of the MTMs particles but also on the direction along which an electromagnetic wave propagates. Therefore, incident condition (angle, polarization, etc.) becomes one of the most important factors to decide the EM

Received 11 January 2017, Accepted 8 June 2017, Scheduled 18 July 2017

* Corresponding author: Chunlin Ji (chunlin.ji@kuang-chi.org).

¹ Shenzhen Kuang-Chi Institute of Advanced Technology, Shenzhen, China. ² Department of Mathematics, Hong Kong Baptist University, Kowloon, Hong Kong, China.

performance of MTMs. As a result, anisotropy would bring additional difficulties in modeling the functional response which leads to non-uniformity between the constitutive parameters [10–12]. Yet the effective medium method assumes the constitutive parameters to be constants, i.e., neglects the discrepancies in frequency responses caused by variation of incident angle and thus leads to poor accuracy of approximation at oblique incidence. Meanwhile, to guarantee the success of an effective medium method, the ratio of operating wavelength to unit cell size must be greater than 4 [13]. Yet optical transformation MTMs usually requires much more complex structures and much larger overall size [5] because the constitutive parameters are often spatially inhomogeneous and anisotropic [14, 15].

An equivalent circuit method was also adopted in modeling MTMs frequency response, in which a predefined circuit is constructed according to the metallic microstructure topology [16–18]. Values of circuit elements were obtained by fitting the frequency response. This approach allows high coherence in predicting the frequency dispersion of MTMs [17, 18]. For example, as well known in radio frequency engineering, the resonance frequency of an equivalent circuit is inversely proportional to the square root of the product of inductance and capacitance. Once the equivalent circuit is configured, the resonance of a system can be fine-tuned by changing the geometrical parameters of microstructures to search optimized circuit parameters. However, synthesis of such a circuit often fails when the complexity of the MTMs unit cell increases, since defining an equivalent circuit becomes very challenging and it hardly converges when fitting its parameters. Once again, these techniques are only proved to succeed at normal incidence or require homogeneity and isotropy of the metamaterial architecture thus contributing little to MTMS rapid design.

To relieve the computing burden of a time-consuming design process, statistical techniques like meta-models (a.k.a. surrogate models, response surface, etc.) were employed to build a mathematical expression to predict the frequency response at unobserved independent variables of the MTMs based on a considerably smaller number of historical simulation data [6]. For example, the spatial distribution of the refractive indices can be determined via a simple polynomial-like regression model [5]. To deal with more sophisticated data in which non-stationarity and/or discontinuities were embedded, a more flexible modeling scheme, Bayesian nonparametric, was utilized to predict the constitutive parameters for any specific design over a diverse range of MTMS particles [6]. These two works save a great amount of time compared to the two conventional approaches. But the prediction of the frequency still relies on representing the refractive index via a particular Drude/Lorentz-type model. Thus, a prompt solution is required to address the spatial dispersion induced by the variation of incident angle.

In this paper, we propose a two-stage surrogate approach to incorporate the aforementioned dispersion induced by the variety of incidence. In Stage I, we represent a different equivalent circuit model, whose values were analytical solutions to a series of rational functions [19]. Since the equivalent circuit is obtained by approximating the functional response itself rather than accommodating a particular MTMs geometrical pattern, the reliability of the circuit is no longer limited by the complexity of the microstructure. The vector-fitting (VF) algorithm is first applied to fit the response of MTMs to a rational function [20, 21]. Then the elements of the equivalent circuits are synthesized by a couple of fractional terms and their poles and residues. After we decompose the functional response to a set of parameters of the equivalent circuits, we can apply a surrogate model, in Stage II, to find the latent input (physical settings)-output (circuit parameters) relations. We utilize the Gaussian process (GP) as the regression approach because it is not only powerful in dealing with multivariate nonlinear data and graphics, but also capable of modeling many physical phenomenon [22]. With this two-stage modeling approach, we implement mapping the relationship between any types of physical settings of MTMs designs to their frequency response.

The structure of this paper is as follows. Section 2 presents the two-stage model, which includes the basic formulations of rational approximation, synthesis of an equivalent circuit representation of such fractional functions, and the GP-based regression model. Section 3 gives the computer experiment results conducted on two metamaterial prototypes to demonstrate the efficiency and accuracy of the proposed approach. We draw the final conclusion in Section 4.

2. METHODOLOGY

2.1. Stage I: Equivalent Circuit Model via Rational Approximation

In this stage, the frequency responses, $F(s)$, of MTMs were presented with fractional functions in the form of

$$F(s) = \sum_{k=1}^n \frac{res_k}{(s - p_k)} + d + sh, \quad (1)$$

with $s = j\omega$ being the complex frequency, res_k and p_k being the k th residue and pole, respectively, which are either real quantities or come in complex conjugate pairs [23, 24]. The real valued constant term d and s -proportional term h are optionally included in the formula. Fitting of this rational function can be well achieved by the vector-fitting algorithm, which approximates the reference data with a few discrete parameters (poles and residues, etc.). We adopt these partial fractions to model the frequency response, since it allows accurate representation of distinct resonances, which always exists in MTMs functional data and cannot be well described by polynomials or splines. In particular, poles obtained via this technique have direct correspondence to resonant peaks of the response data, which offers quick identification to the dispersive properties of MTMs, as the resonant frequency equals 2π of the absolute value of the imaginary part of each pole.

Before the synthesis of equivalent circuits, we must choose a certain representation form to the reflection and/or transmission performance of an MTMs system. The candidates include S -parameter, characteristic impedance, and transfer matrix, to name a few. Without losing any generality, we aim to approximate admittance parameters and calculate the circuit element values once the pole and residue pairs are known. Compared to the conventional equivalent circuits, the model adopted in this work is rather fixed, where only two types of networks, namely, the series RL and lumped RLC , are used to formulate the circuit, although the microstructure patterns vary from case to case. These two building blocks of the fixed circuit model are depicted in Figures 1(a) and (b), respectively. In a fixed circuit, each series RL loop corresponds to a real pair of pole and residue, whereas each lumped RLC network deals with the complex pair, which helps to understand the working principle of the MTMs composite. As the order of vector fitting increases, we establish the circuit by adding more parallel loops of series structures in accordance to the number of real poles, N_r , and lumped RLC counterparts agree with the number of complex pairs, N_C . Examples of such circuit configuration are shown in Figure 6.

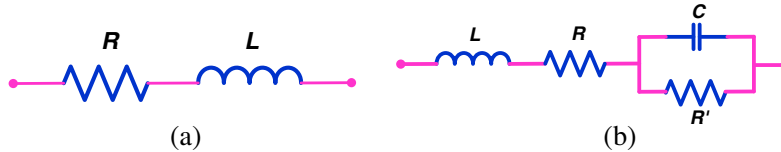


Figure 1. (a) Equivalent RL circuit for real pole synthesis; (b) Equivalent lumped RLC circuit for a complex pole.

2.1.1. Real Poles

As shown in Figure 1(a), the real pole and residue pair of function $F(s)$ is synthesized by series RL , the values of which are

$$L = \frac{1}{res_R} \text{ and } R = -\frac{p_R}{res_R} \quad (2)$$

where p_R and res_R are real poles extracted by VF procedure.

2.1.2. Complex Poles Pairs

Let p_1, p_2, res_1 and res_2 be pairs of complex and conjugate poles and residues, respectively. We can obtain the following circuit parameters:

$$\begin{aligned}
L &= \frac{1}{res_1 + res_2} \\
R &= \frac{1}{res_1 + res_2} \times \left[-(p_1 + p_2) + \frac{1}{res_1 + res_2} (res_1 p_2 + res_2 p_1) \right] \\
C &= \frac{res_1 + res_2}{p_1 p_2 + [-(p_1 + p_2) + \frac{1}{res_1 + res_2} (res_1 p_2 + res_2 p_1)]} \times \left(\frac{res_1 + res_2}{res_1 p_2 + res_2 p_1} \right). \\
R' &= -\frac{1}{C} \frac{(res_1 + res_2)}{(res_1 p_2 + res_2 p_1)}
\end{aligned} \tag{3}$$

If term d and h are included, they are synthesized with a resistance and a conductance, whose values are $1/d$ and h , respectively. More detailed methodology and expressions for equivalent circuit synthesis are presented in [19].

2.2. Stage II: Gaussian Process Regression

In this stage, values of equivalent circuit elements are used as training observations (or say response variables), and the physical settings of microstructures act as independent variables. The problem can be described as follows, and for each circuit element, the data are given as $D = \{(x_i, y_i)_{i=1}^N\}$, where $x_i \in X = R^G$, $Y = R$, N is the number of data points and G the dimensionality of input vectors. The purpose is to find a regression function $g(x)$ to relate the observations to the input variables. However, instead of generating a single regression function, it transductively provides a posterior density over target values for the training and test set [22].

To fully define a GP, both its mean function $m(x)$ and the covariance function $k(x, x')$ should be specified as

$$g(x) \sim GP(m(x), k(x, x')). \tag{4}$$

In general, the covariance function can take any form of a function that generates a nonnegative definitive covariance matrix K between any two arguments. The choice of the covariance function implicitly assumes certain aspects of the underlying process, such as smoothness, periodicity, and stationary, which can be fine-tuned for special applications like our case. Among all possible candidates, the squared exponential covariance function is most commonly adopted, given by

$$k(x, x') = \sigma_\nu^2 \exp\left(\sum_\nu \frac{1}{2l_\nu^2} |x - x'|^2\right), \tag{5}$$

which is parameterized by two parameters σ_ν^2 , called signal variance, and l_ν named characteristic length scale. These two parameters are categorized as hyper parameters in the Bayesian statistics community. The signal variance controls the range of magnitude that the function value can vary. And the characteristic length scale, loosely speaking, can be thought of as the required distance, away from a given point to cause a significant change in the function value in the input space. We denote the union of hyperparameters by γ , whose values are evaluated by optimizing the log marginal likelihood:

$$\log p(y | X, \gamma) = -\frac{1}{2} y^T K^{-1} y - \frac{1}{2} \log |K| - \frac{n}{2} \log 2\pi. \tag{6}$$

Here, we assume a noise-free electromagnetic response obtained via numerical simulation. Then the covariance matrix K for y is identical to that of the noise-free latent function $g(x)$.

By evaluating the mean and covariance matrix, predictive response y^* of new input X^* can be sampled from the joint posterior distribution as

$$y^* | X^*, X, y \sim N\left(K(X^*, X) K(X, X)^{-1}\right) y, K(X^*, X^*) - K(X^*, X) K(X, X)^{-1} K(X, X^*), \tag{7}$$

where $N(a, b)$ denotes the Gaussian density function with mean a and covariance b , and $K(A, B)$ denotes the matrix of covariance evaluated at each pair of points coming from both involved data sets, A and

B. Once the GP models are established, predictions at unobserved input sites can be generated by Bayesian statistics [22]. And this marks the completion of our two-stage modeling and design process. We summarize the operations as below:

Stage I: Equivalent Circuit Setups Based Upon Poles and Residues via Rational Approximation

1. Rewrite each reference dataset as a function of discrete parameters as

$$F_i(s) = \varphi(s, \phi_i),$$

where ϕ_i is the combination of poles and residues (d and h as well, if included) at i th input set.

2. Compute the circuit parameters

$$y_{ij} = \eta_j(\phi_i),$$

where y_{ij} is the value j th circuit element at i th input set.

Stage II: Construct GP Regression Models for Each Circuit Element Synthesized via Rational Approximation

$$y_{ij} \sim GP_{ij}(m(x_i), k(x_i, x')).$$

For new design points in the test set, prediction of their frequency responses is straight forward by following the in versed sequence of two stages above, i.e., first predicting the circuit elements with corresponding GP models and then calculating the sum of corresponding fractional functions.

3. EXPERIMENTAL VERIFICATION

In this section, we present the simulation studies of two MTMs prototypes designed with the proposed method to verify its effectiveness and accuracy. The verification contains three major components: data, intermediate results of both stages, and predictive accuracy. We present two prototypes to verify that our approach can be applied to a vast range of topology families of metamaterials.

3.1. Data

Each of the two metamaterial prototypes contains a single microstructure layer made of copper with a thickness of 0.018 mm, and with stratified dielectrics stacked symmetrically on both sides. The relationship between the microstructure and macrostructure of MTMs prototypes is conceptually explained in Figure 2. We aim to relate the design variables of MTMs, i.e., physical dimensions, to the EM performance. Meanwhile, the incident angle, denoted by θ , should be included as an independent variable in our model. The incident angle is defined as the angle between the incident wave vector,

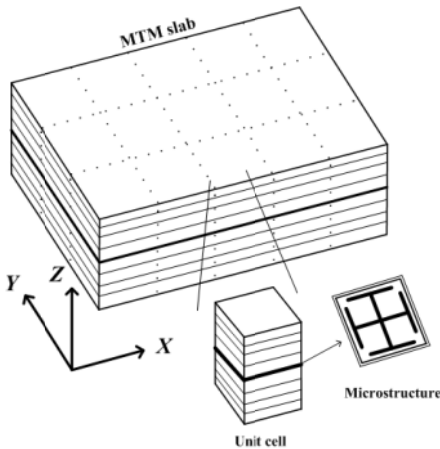


Figure 2. Layout of microstructure and macrostructure.

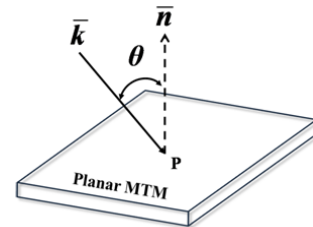


Figure 3. Illustration of an EM wave incident onto a MTM slab.

\bar{k} , and plane normal, \bar{n} , shown in Figure 3. Therefore, both input spaces of the two examples are two-dimensional. The training sets of both prototypes are obtained via full-wave simulation. And for each prototype, we compare the predictions of our approach to simulation results at the same given test sets to demonstrate the accuracy.

3.2. Prototype I

3.2.1. Training Set

The pattern of Prototype I is generated from the well-known Jerusalem cross and modified by adding a square coil along the edges of the unit cell [25]. The microstructure is parameterized by a geometric variable, \mathbf{w} , as illustrated in Figure 4(a). The values of \mathbf{w} of the training set are from 0.6 mm to 1.4 mm by an interval of 0.2 mm. Meanwhile, at each setting of \mathbf{w} , we also take a sweep on θ , with $0 \text{ deg} \leq \theta \leq 45 \text{ deg}$, by an interval of 5 degree. As a result, there are 50 data points in the training set. Other constant geometric dimensions are also marked in Figure 4(a). For all dielectrics, we assume unity permeability (i.e., $\mu = 1$) permittivity ε , and thickness t which are listed in Table 1.

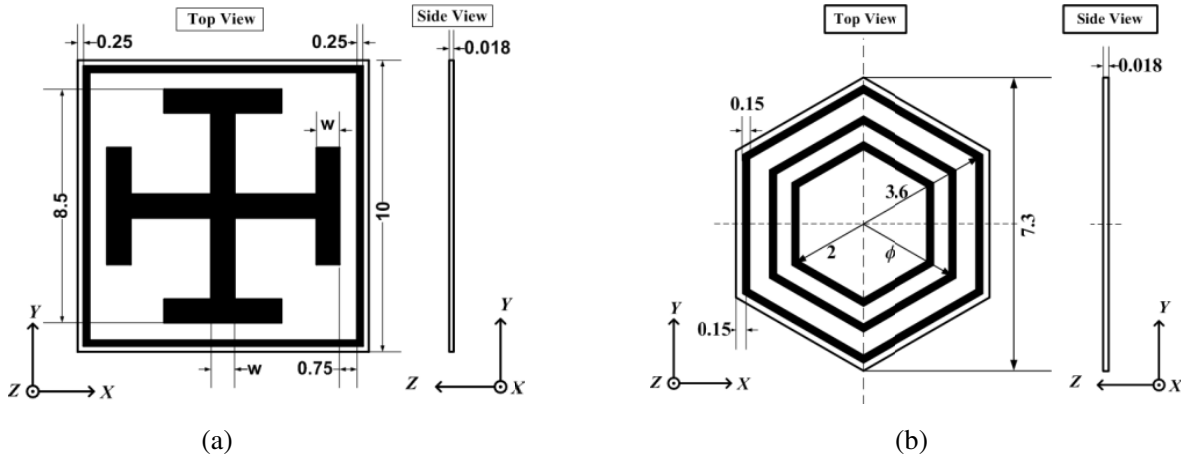


Figure 4. Illustration of two MTM prototypes: (a) Parametric presentation of the modified Jerusalem cross; (b) Parametric presentation of the triple hexagonal rings.

Table 1. Material properties of prototype 1.

	ε	μ	t
LT1	3.15-j1.575E-2	1	0.75
LT2	2.7-j1.755E-2	1	0.1
LT3	1.05-j1.575E-2	1	1
LT4	2.7-j1.755E-2	1	0.1
Microstructure			
LB4	2.7-j1.755E-2	1	0.1
LB3	1.05-j1.575E-2	1	1
LB2	2.7-j1.755E-2	1	0.1
LB1	3.15-j1.575E-2	1	0.75

Table 2. Material properties of prototype 2.
* LT-layer on top; LB-layer on the back.

	ε	μ	t
LT1	3.15-j1.575E-2	1	2.5
LT2	1.09-j0.71E-2	1	1.5
LT3	3.15-j1.575E-2	1	1
Microstructure			
LB3	3.15-j1.575E-2	1	1
LB2	1.09-j0.71E-2	1	1.5
LB1	3.15-j1.575E-2	1	2.5

3.2.2. Test Set

We sweep the geometric dimension parameter \mathbf{w} from 0.7 mm to 1.3 mm by an interval of 0.2 mm, while θ is swept from 2 to 44 degree by an interval of 2 degree. In total, 92 data points form the test set.

3.3. Prototype II

3.3.1. Training Set

We present a different metamaterial prototype whose topology is depicted in Figure 3(b). The microstructure consists of three hexagonal loops, where two of them are fixed and the other with varying physical dimension. The geometric variable of the varying hexagonal loop is parameterized by ϕ , whose value is from 2.1 mm to 2.5 mm by an interval of 0.2 mm. Properties of dielectrics in this MTM structure are given in Table 2. Again, we also include incident angle as one input variable, with $0 \text{ deg} \leq \theta \leq 70 \text{ deg}$, by an interval of 5 degrees. In total, all possible variations of inputs add up to 45 total points.

3.3.2. Test Set

We predict the EM performance of designs with geometric parameter ϕ from 2.2 mm and 2.4 mm, while θ is swept from 0 to 70 degree by an interval of 2 degree. In total, the test set contains 72 data points. The data set formations of both prototypes are concluded in Table 3.

Table 3. Dataset configuration of both metamaterial prototypes.

	Training set	Test set
Prototype I	50 points with $\mathbf{w} \in [0.6 : 0.2 : 1.4]$ and $\theta \in [0 : 5 : 45]$	92 points with $\mathbf{w} \in [0.7 : 0.2 : 1.3]$ and $\theta \in [0 : 2 : 45]$
Prototype II	45 points with $\phi \in [2.1 : 0.2 : 2.5]$ and $\theta \in [0 : 5 : 70]$	72 points with $\phi \in [2.2, 2.4]$ and $\theta \in [0 : 2 : 70]$

3.4. Results

3.4.1. Stage I: Vector Fitting and Equivalent Circuit Modeling

For our first MTM prototype, we fit the simulated frequency response with 3 poles (one real pole and one complex pair) to approximate each admittance curve. The statistic used for comparison of fitting accuracy is root mean-square error (*RMSE*):

$$MSE = \sum_{j=1}^{n_s} \left(F_j^{fit}(s) - F_j(s) \right)^2 / n_s \text{ and } RMSE = \sqrt{MSE}, \quad (8)$$

where $F_j^{fit}(s)$ and $F_j(s)$ are the model predicted response and full-wave simulation results at j th test point, respectively. n_s is the number of responses at each test input, which equals one thousand in our case. With the proposed number of poles, we can achieve very high accuracy with the approximation error less than 0.002. A comparison of the approximated result (red circles) and reference data (blue dash) is shown in Figures 5(a) and (b). The deviations between these two are presented by the black solid curves. Corresponding to the curves, Table 4 lists the combination of extracted quantities of the approximation as an example.

Table 4. Example of extracted parameters of Prototype I via vector fitting.

Poles	Residues
$-1.26\text{E} + 07$	$2.21\text{E} + 08$
$-3.42\text{E} + 08 + j5.58\text{E} + 10$	$1.65\text{E} + 08 + j5.72\text{E} + 06$
$-3.42\text{E} + 08 - j5.58\text{E} + 10$	$1.65\text{E} + 08 - j5.72\text{E} + 06$
d: $2.24\text{E} - 05$	h: $2.11\text{E} - 14$

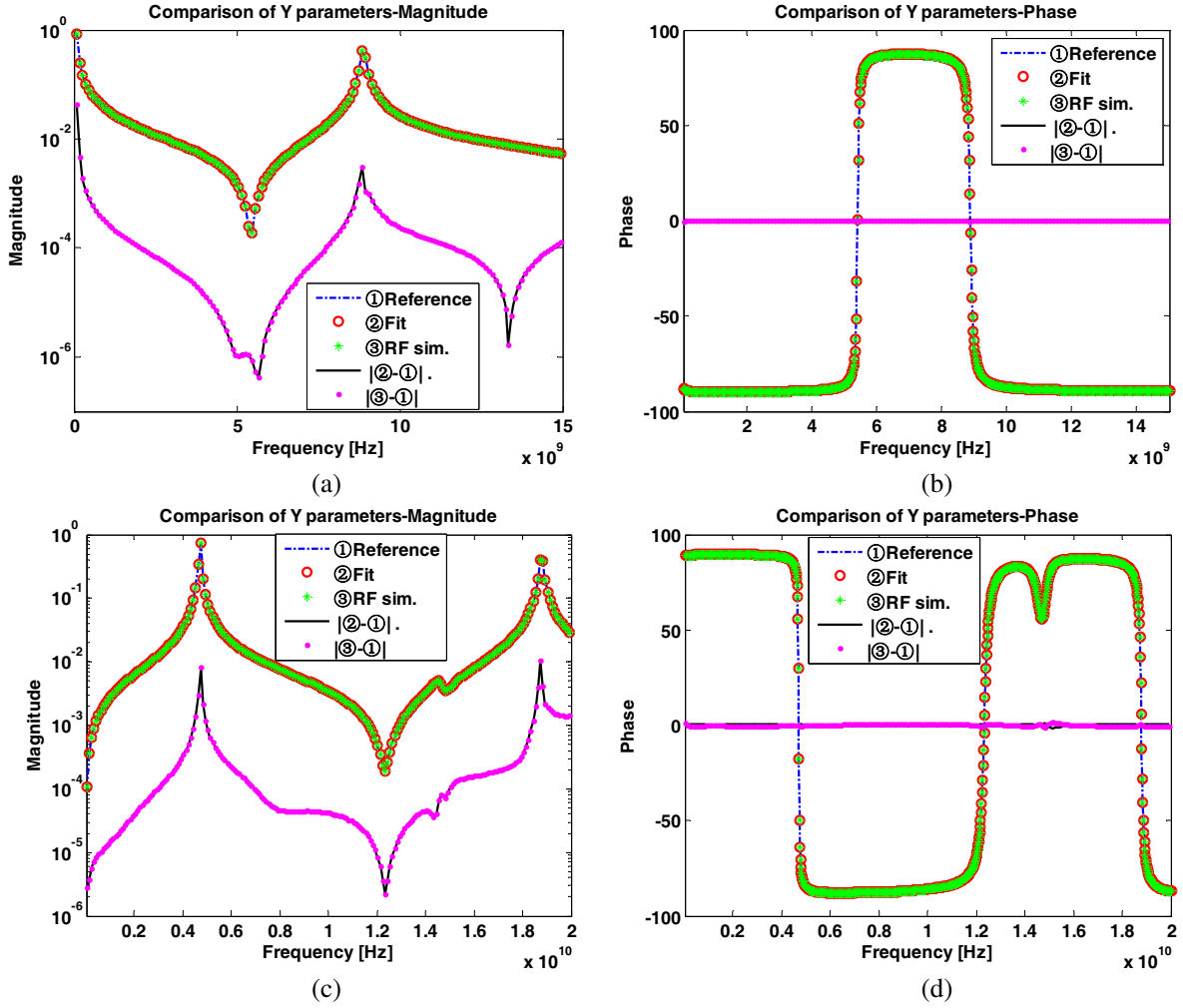


Figure 5. Comparison of rational approximation and equivalent circuits simulation to reference data: (a) Prototype I Magnitude; (b) Prototype I Phase; (c) Prototype II Magnitude; (d) Prototype II Phase.

We present the results in Stage I of Prototype II in the same manner, where the example of pole-residue pairs is listed in Table 5. In contrast to Prototype I, functional responses of Prototype II are approximated by 6 poles (3 complex pairs), plus term d and h , while similar approximation accuracy is achieved, shown in Figures 5(c) and (d). Corresponding pole-residue pairs are listed in Table 5.

Table 5. Example of extracted parameters of Prototype II via vector fitting.

Poles	Residues
$-1.41\text{E} + 08 + \text{j}2.94\text{E} + 10$	$1.65\text{E} + 08 + \text{j}2.57\text{E} + 06$
$-1.41\text{E} + 08 - \text{j}2.94\text{E} + 10$	$1.65\text{E} + 08 - \text{j}2.57\text{E} + 06$
$-1.33\text{E} + 09 + \text{j}9.22\text{E} + 10$	$3.15\text{E} + 08 + \text{j}1.41\text{E} + 05$
$-1.33\text{E} + 09 - \text{j}9.22\text{E} + 10$	$3.15\text{E} + 08 - \text{j}1.41\text{E} + 05$
$-4.06\text{E} + 08 + \text{j}1.18\text{E} + 11$	$2.08\text{E} + 08 + \text{j}2.20\text{E} + 06$
$-4.06\text{E} + 08 - \text{j}1.18\text{E} + 11$	$2.08\text{E} + 08 - \text{j}2.20\text{E} + 06$
$d: 1.51\text{E} - 04$	$h: 9.72\text{E} - 15$

After the rational approximation of the response, we convert the parameters of fractional functions to values of equivalent circuit elements. For both prototypes, the equivalent circuit and values of elements corresponding to frequency response in Figure 5 are displayed in Figure 6. The equivalent circuit extracted from the quantities of vector fitting is SPICE compatible [19]. We take the synthesized equivalent circuits to RF circuit simulation software and compare the simulation data (green star dash) to the reference (blue curves), with the deviation also included (magenta circles). Notice regression should also be performed to the constant term d and s-proportional term h , although not shown in Figure 6.

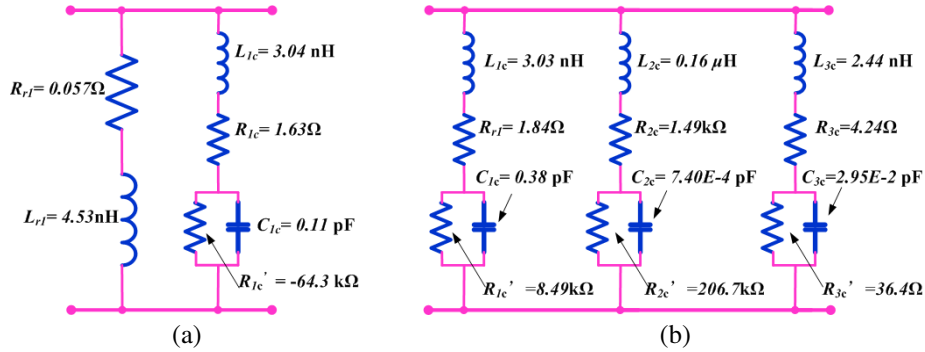


Figure 6. Equivalent circuits with example of element values: (a) Prototype I; (b) Prototype II.

3.4.2. Stage II: Gaussian Processes Regression

We view the values of equivalent circuit elements as observations for GP regressions and build separate GP models for different elements in the equivalent circuit. In our case, we obtain 8 regression surfaces for Prototype I and 14 surfaces for Prototype II, one for each element. This seems too much to run with a computer code. In fact, building a single GP regression model and accomplishing Bayesian inference only take a few seconds. The time efficiency of the proposed method is displayed in Section 3.3. The exponential square covariance function was adopted, and the optimized hyper-parameters for both prototypes are given in Table 6. Meanwhile, a smooth regression surface of inductor L , in the lumped RLC loop, against the input variables of Prototype I is displayed in Figure 7.

Table 6. Example of hyperparameters learnt in a GP for Prototype I.

Signal variances	Characteristic lengthscales
$\sigma_1^2 = 0.001$ and $\sigma_2^2 = 0.001$	$l_1 = 2.02$ and $l_2 = 19.99$

3.5. Efficiency and Accuracy

Our control data for the test sets were obtained by running full-wave simulations performed on a desktop computer with Intel Core i7-2600 central processing units (CPUs) and 8 GB of random access memory (RAM). We conclude time consumed for the full-wave simulations and that of our approach, which are both listed in Table 7, which demonstrates time-efficiency of our method.

To illustrate the predictive accuracy of our approach, examples of the compared results of magnitude and phase of reflection (S_{11}) and transmission (S_{21}) of the proposed method to that via full-wave simulation are depicted in Figure 8. Here, we only demonstrate fitting the frequency response in polarization of the TE mode, while the proposed modeling scheme is also adaptable to the TM mode.

We conclude the predictive accuracy of both metamaterial prototypes of the proposed approach in Table 8. The proposed approach allows accurate approximation, with the average RMSE less than 0.05 for both metamaterial prototypes, which should be satisfactory for many engineering applications.

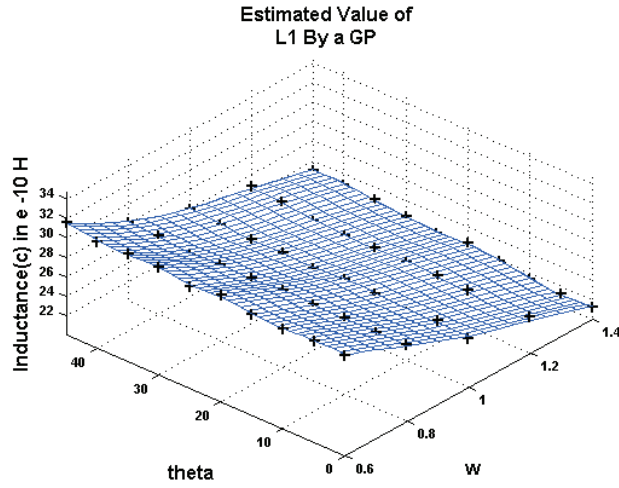


Figure 7. Example of Gaussian process regression surface.

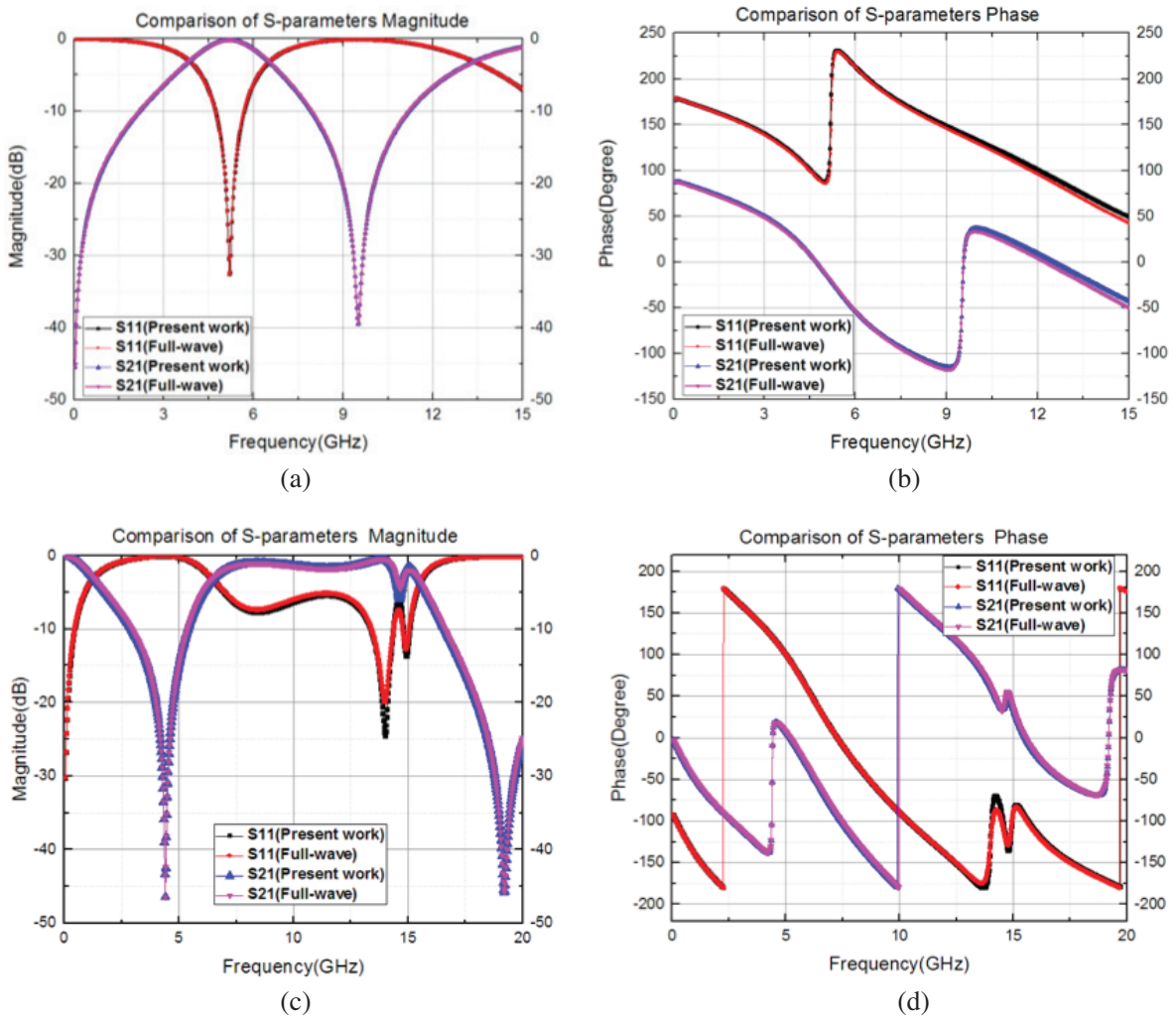


Figure 8. Comparison of S -parameters of the proposed method and simulation results: (a) Prototype I Magnitude; (b) Prototype I Phase; (c) Prototype II Magnitude; (d) Prototype II Phase.

Table 7. Time consumption of full-wave simulation and the present work.

	Full-wave simulation	Present work
Prototype I	> 160 Hours	< 3 Minutes
Prototype II	> 130 Hours	< 3 Minutes

Table 8. Predictive accuracy of proposed approach on both prototypes.

	Min	1st Qu.	Median	Mean	3rd Qu.	Max.
Prot. I S_{11}	0.0243	0.0347	0.0449	0.0451	0.0551	0.0651
Prot. I S_{21}	0.0191	0.0261	0.0323	0.0325	0.0395	0.0463
Prot. II S_{11}	0.0336	0.0413	0.0466	0.0471	0.0539	0.0608
Prot. II S_{21}	0.0314	0.0370	0.0417	0.0421	0.0483	0.0539

4. CONCLUSION

This work presents a novel two-stage method to model the frequency response of MTMS and aids the design process. With our approach, we break down the complex modeling problem to a VF-based equivalent circuit modeling process and a GP regression process. This two-stage method can easily generate the mapping function from any types of independent variables, including geometric dimensions and incident angle to their corresponding EM responses. The predictive property of this model enables the massive reduction of time-consuming simulations. As the experimental results demonstrated, this proposed modeling scheme can facilitate the rapid design of MTMs with high accuracy in the prediction of the EM response of various MTMs microstructures.

ACKNOWLEDGMENT

This work was supported by Shenzhen Key Laboratory of Artificial Microstructure Design (Grant No. CXB201109210099A), Guangdong Key Laboratory of Meta-RF Microwave Radio Frequency (Grant No. 2011A060901010), Guangdong Natural Science Funds for Distinguished Young Scholar (Grant No. S20120011253), Shenzhen Science and Technology Plan (Grant No. JCYJ20151015165557141) and Shenzhen Science and Technology Plan (Grant No. JSGG20150917174852555).

REFERENCES

1. Shelby, R. A., D. R. Smith, and S. Schultz, "Experimental verification of a negative index of refraction," *Science*, Vol. 292, 77-9, Apr. 6, 2001.
2. Eleftheriades, G. V. and K. G. Balmain, *Negative-refraction Metamaterials: Fundamental Properties and Applications*, J. Wiley, Hoboken, NJ, ISBN: 978-0471744757, 2005.
3. Marqués, R., F. Martín, and M. Sorolla, "Metamaterials with Negative Parameters: Theory, Design and Microwave Applications", John Wiley & Sons, ISBN: 978-0-471-74582-2, 2011.
4. Cui, T. J., D. Smith, and R. Liu, *Metamaterials: Theory, Design, and Applications*, Springer, New York, NY, ISBN: 978-1441905734, 2014.
5. Liu, R., C. Ji, J. J. Mock, J. Y. Chin, T. J. Cui, and D. R. Smith, "Broadband ground-plane cloak," *Science*, Vol. 323, 366-9, 2009.
6. Liu, B. and C. Ji, "Bayesian nonparametric modeling for rapid design of metamaterial microstructures," *International Journal of Antennas & Propagation*, Vol. 2014, 187-187, 2014.

7. Smith, D. R., S. Schultz, P. Markoš, and C. M. Soukoulis, "Determination of effective permittivity and permeability of metamaterials from reflection and transmission coefficients," *Physical Review B*, Vol. 65, 195104, 2001.
8. Chen, X., T. M. Grzegorzcyk, B. I. Wu, P. J. Jr, and J. A. Kong, "Robust method to retrieve the constitutive effective parameters of metamaterials," *Physical Review E Statistical Nonlinear & Soft Matter Physics*, Vol. 70, 811–811, 2004.
9. Menzel, C., C. Rockstuhl, T. Paul, F. Lederer, and T. Pertsch, "Retrieving effective parameters for metamaterials at oblique incidence," *Physical Review B*, Vol. 77, No. 19, 195328-1–195328-8, 2008.
10. Rahm, M., D. Roberts, J. Pendry, and D. Smith, "Transformation-optical design of adaptive beam bends and beam expanders," *Optics Express*, Vol. 16, 11555–11567, 2008.
11. Rahm, M., D. Schurig, D. A. Roberts, S. A. Cummer, D. R. Smith, and J. B. Pendry, "Design of electromagnetic cloaks and concentrators using form-invariant coordinate transformations of Maxwell's equations," *Photonics and Nanostructures-fundamentals and Applications*, Vol. 6, 87–95, 2008.
12. Schurig, D., J. Mock, B. Justice, S. A. Cummer, J. B. Pendry, A. Starr, et al., "Metamaterial electromagnetic cloak at microwave frequencies," *Science*, Vol. 314, 977–980, 2006.
13. Koschny, T., P. Marko, E. N. Economou, D. R. Smith, D. C. Vier, and C. M. Soukoulis, "Impact of inherent periodic structure on effective medium description of left-handed and related metamaterials," *Physical Review B*, Vol. 71, 5105, 2005.
14. Li, J. and J. Pendry, "Hiding under the carpet: A new strategy for cloaking," *Physical Review Letters*, Vol. 101, 203901, 2008.
15. Jiang, W. X., J. Y. Chin, Z. Li, Q. Cheng, R. Liu, and T. J. Cui, "Analytical design of conformally invisible cloaks for arbitrarily shaped objects," *Physical Review E*, Vol. 77, 066607, 2008.
16. Bilotti, F., A. Toscano, L. Vegni, and K. Aydin, "Equivalent-circuit models for the design of metamaterials based on artificial magnetic inclusions," *IEEE Transactions on Microwave Theory & Techniques Mtt*, Vol. 55, 2865–2873, 2007.
17. Chen, H., L. Ran, J. Huangfu, T. M. Grzegorzcyk, and J. A. Kong, "Equivalent circuit model for left-handed metamaterials," *Journal of Applied Physics*, Vol. 100, 024915-024915-6, 2006.
18. Gil, I., J. Bonache, J. Garcia-Garcia, and F. Martin, "Tunable metamaterial transmission lines based on varactor-loaded split-ring resonators," *IEEE Transactions on Microwave Theory & Techniques*, Vol. 54, 2665–2674, 2006.
19. Antonini, G., "SPICE equivalent circuits of frequency-domain responses," *IEEE Transactions on Electromagnetic Compatibility*, Vol. 45, 502–512, 2003.
20. Majumdar, P., Z. Zhao, Y. Yue, C. Ji, and R. Liu, "Equivalent circuit model of cross and circular ring FSS using vector fitting," *2014 3rd Asia-Pacific Conference on Antennas and Propagation (APCAP)*, 1042–1045, 2014.
21. Majumdar, P., Z. Zhao, Y. Yue, C. Ji, and R. Liu, "Equivalent circuit model of different configurations of loop elements using vector-fitting," *PIERS Proceedings*, 2395–2399, Guangzhou, Aug. 25–28, 2014.
22. Williams, C. K. and C. E. Rasmussen, *Gaussian Processes for Machine Learning*, MIT Press, ISBN 0-262-18253-X, 2006.
23. Semlyen, A. and B. Gustavsen, "Vector fitting by pole relocation for the state equation approximation of nonrational transfer matrices," *Circuits, Systems and Signal Processing*, Vol. 19, 549–566, 2000.
24. Gustavsen, B. and A. Semlyen, "Rational approximation of frequency domain responses by vector fitting," *IEEE Transactions on Power Delivery*, Vol. 14, 1052–1061, 1999.
25. Munk, B., *Frequency Selective Surfaces: Theory and Design*, J. Wiley, Hoboken, NJ, ISBN 978-0-471-37047-5, 2005.